Materials Science-Poland, Vol. 24, No. 4, 2006

FMR study of nanocarbon materials obtained by carburisation of nanocrystalline iron

U. NARKIEWICZ[1*], W. ARABCZYK[1], I. PEŁECH[1], N. GUSKOS[2, 3], J. TYPEK[3], M. MARYNIAK[3], M. J. WOŹNIAK[4], H. MATYSIAK[4], K. J.KURZYDŁOWSKI[4]

[1]Institute of Chemical and Environment Engineering, Szczecin University of Technology, Pułaskiego 10, 70-322 Szczecin, Poland

[2]Solid State Section, Department of Physics, University of Athens, Panepistimiopolis, 157 84 Zografos, Greece

[3] Institute of Physics, Szczecin University of Technology, al. Piastów 17, 70-310 Szczecin, Poland

[4]Faculty of Materials Science and Engineering, Warsaw University of Technology, Wołoska 141, 02-507 Warsaw, Poland

Samples of nanocrystalline iron were carburised with ethylene and next reduced with hydrogen. Both carburisation and reduction were monitored by the thermogravimetry. The obtained samples were characterised using X-ray diffraction, high-resolution transmission electron microscopy and ferromagnetic resonance. The samples after carburisation contained cementite (Fe_3C) and carbon deposit (nanofibres and nanotubes). As the result of reduction with hydrogen at 450 or 500 °C cementite was reduced to iron. A major part of carbon was also hydrogenated, only thin carbon nanotubes remained. The FMR spectra of the prepared samples were recorded at room temperature. The sample after carburisation has shown a wide FMR line with weak intensity while the resonance field has been shifted to lower magnetic field. This spectrum has been attributed to the presence of cementite. The FMR lines corresponding to samples after reduction are more intense and are connected with the presence of α-Fe nanoparticle conglomerates.

Key words: *carburisation; reduction; iron carbide; FMR; HRTEM*

1. Introduction

Iron carbide-based nanoparticles are of growing interest due to their improved magnetic properties as well as potential application in catalysis, sensors and reduction of the cost required to produce bulk quantities [1–5]. In particular, nanocomposites

*Corresponding author, e-mail: urszula.narkiewicz@ps.pl

containing iron carbide (Fe_3C) are suited to diverse technological applications due to their enhanced mechanical properties [6] and importance in ferrous metallurgy [7]. Fe_3C nanoparticles were found to be more resistant to oxidation than α-Fe nanoparticles due to formation of carbonaceous layers on the particle surfaces [1, 2]. Many preparative methods to obtain iron carbide and carbon materials are known, among them the effective one is chemical vapour deposition (CVD) with application of transition metal catalysts [8–11]. Usually, the CVD method generates different forms of carbon, like, e.g., amorphous carbon, carbon fibres or nanotubes. To remove amorphous carbon many methods have been used [12–14] and among them the hydrogenation process carried out at 900 °C [15]. The ferromagnetic resonance (FMR) method can be very useful for investigation of the magnetic interaction and concentration of magnetic nanoparticles (especially iron carbide and α-Fe) and their magnetic interaction [16–19]. In this work, nanoparticles (iron carbide, α-Fe and nanocarbons) formed during carburisation of nanocrystalline iron with ethylene were studied using X-ray diffraction (XRD) high-resolution transmission electron microscopy (HRTEM) and FMR methods.

2. Experimental

Nanocrystalline iron was obtained by fusion of magnetite with small amounts of promoter oxides (Al_2O_3 and CaO), followed by reduction with hydrogen. The material obtained after the fusion was crushed and sieved to obtain a fraction in the range 1.2–1.5 mm and then reduced with hydrogen according to a procedure described previously [20]. After reduction, nanocrystalline iron was obtained and the promoters remained in the oxidised state. To avoid rapid oxidation on contact with air, the samples were passivated under nitrogen containing traces of oxygen. The chemical composition of the obtained samples was characterised by the AES-ICP method (Yvon –Jobin). Besides iron, the samples contained 2.9% of Al_2O_3 and 3.0% of CaO. The role of two promoter oxides was to stabilize the nanocrystalline iron structure against sintering. The phase composition of the samples was determined by XRD method (Philips X'Pert); the mean crystal size of iron particles calculated using Scherrer's equation was 17 nm.

The carburisation processes were carried out in the spring thermobalance equipped with a cathetometer. The mass changes were registered with the accuracy of 10^{-4} g. A platinum basket hung in the thermobalance was used to place a single layer of grains.

Before each carburisation, the thin passivation layer of the sample was removed by reducing polythermally under hydrogen (40 dm^3/h) at the temperature rising from 20 °C to 500 °C. The carburisation processes were carried out under pure ethylene (40 dm^3/h) under atmospheric pressure at 550 °C. After carburisation, the samples were cooled to room temperature under nitrogen flow. Some carburised samples were treated with hydrogen at the temperatures of 450 °C and 500 °C. The phase composi-

tions of the samples after carburisation, and after carburisation followed by reduction was determined by XRD and their morphology was investigated by HRTEM (Jeol JEM 3010) and atomic force spectroscopy (AFM, Digital Instruments) methods.

Magnetic resonance absorption measurements were carried out with a conventional X-band (ν = 9.43 GHz) Bruker E 500 spectrometer with 100 kHz magnetic field modulation. The samples, each containing around 20 mg of the material, were placed into 4 mm-in-diameter quartz tubes. Prior to the measurements, the samples were magnetized with a steady magnetic field of 1.6 T to saturate any domain structure. The measurements were performed at room temperature.

3. Results and discussion

The sample of nanocrystalline iron was carburised under ethylene at 550 °C until the mass increase of 1.2 g C/g Fe (Sample III). The thermogravimetric (TG) line of the carburisation process is shown in the left part of Fig. 1. According to XRD analysis (upper pattern in Fig. 2), the sample contains two phases: cementite and graphite. In the HRTEM image of the same sample (Fig. 3a), dark agglomerates of iron carbide can be seen, dispersed in carbon. Some carbon fibres are visible and at the end of these oblong carbon forms the crystallites of Fe_3C are located. Besides thick carbon fibres, agglomerates of iron carbides encapsulated with carbon are also visible in the left top corner of the picture. At higher magnification (Fig. 3b), it is seen that the particles of cementite are encapsulated in the shell of 15 nm in thickness, formed by sheets of graphite. Thin multiwall carbon nanotubes can also be observed, about 10 nm in diameter (Fig. 3c).

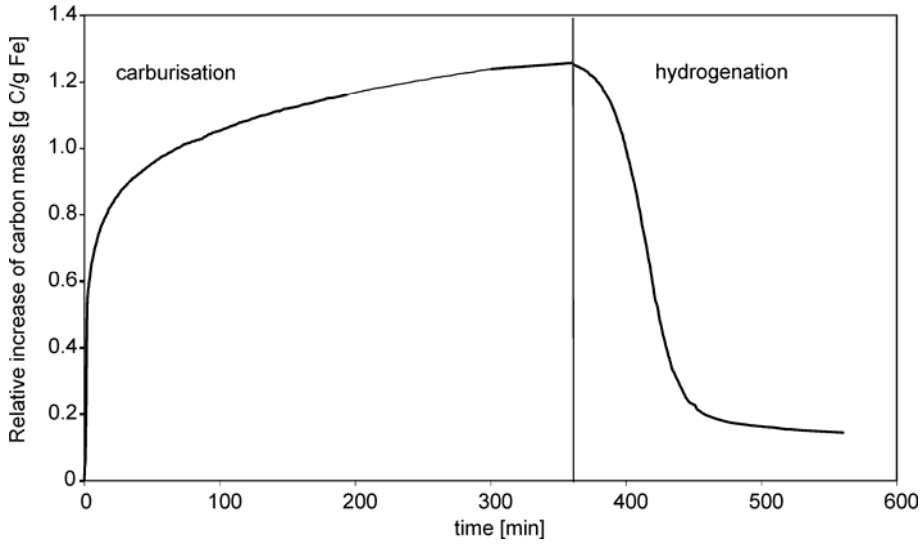

Fig. 1. TG curves of carburisation at 550 °C and reduction at 500 °C

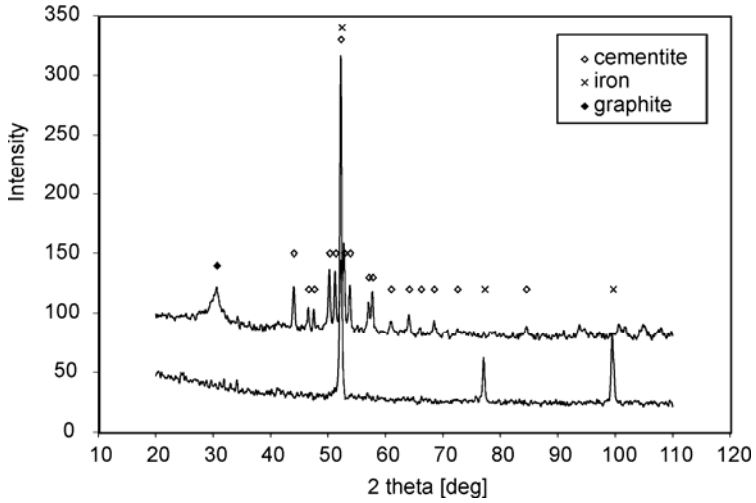

Fig. 2. XRD patterns of the samples: after carburisation at 550 °C (upper spectrum) and after reduction at 450 °C (lower spectrum)

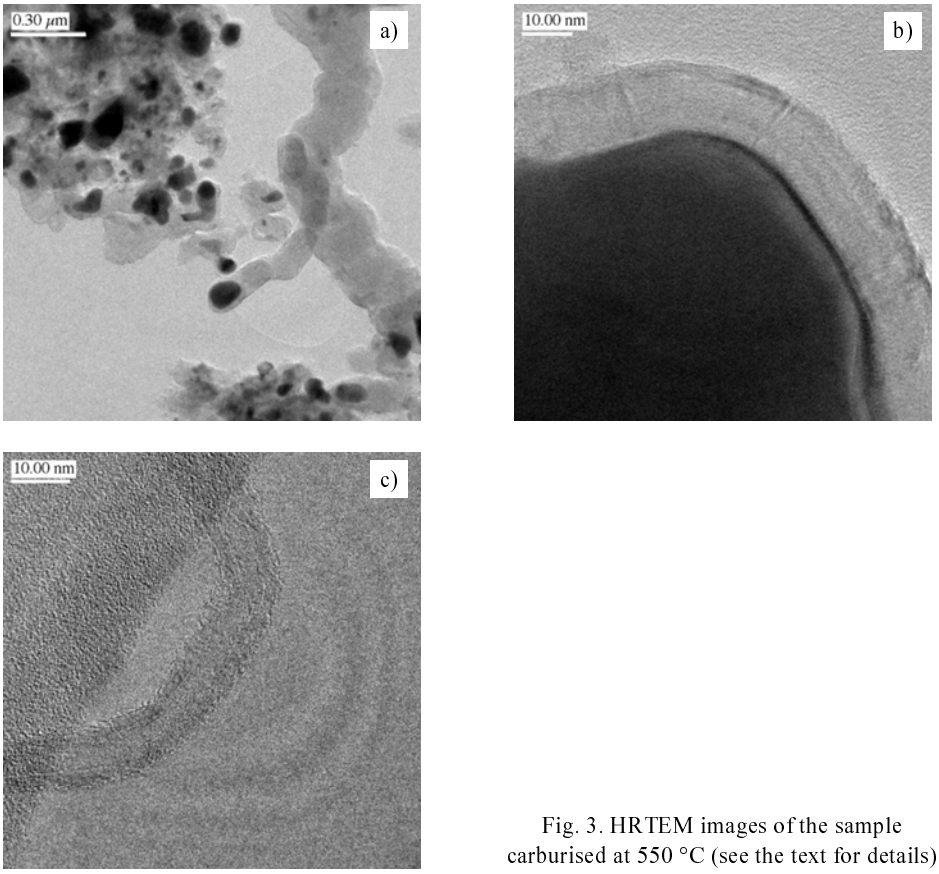

Fig. 3. HRTEM images of the sample carburised at 550 °C (see the text for details)

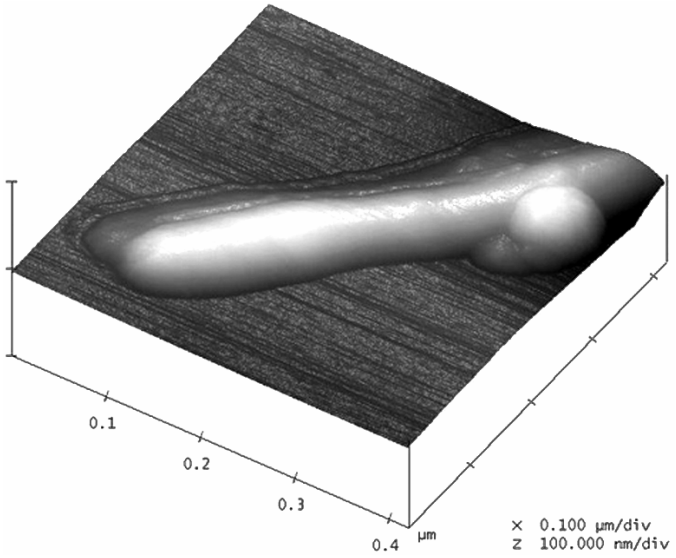

Fig. 4. AFM picture of the carburised sample at 550 °C

In the AFM picture of this sample, some oblong carbon forms can be observed (Fig. 4), below 100 nm in diameter.

The carburised sample was next subject to hydrogenation at 450 °C (sample II). As a result of this process, the carbon content in the sample decreased from 1.2 to 0.4 g C/g Fe. In the XRD pattern of this sample, only the peaks corresponding to α-Fe are observed (lower pattern in Fig. 2). In the HRTEM picture of the sample thick carbon fibres are no more found (Fig. 5a), they should have been removed as a result of hydrogenation. In Figure 5b a multiwall bamboo-shaped nanotube is shown.

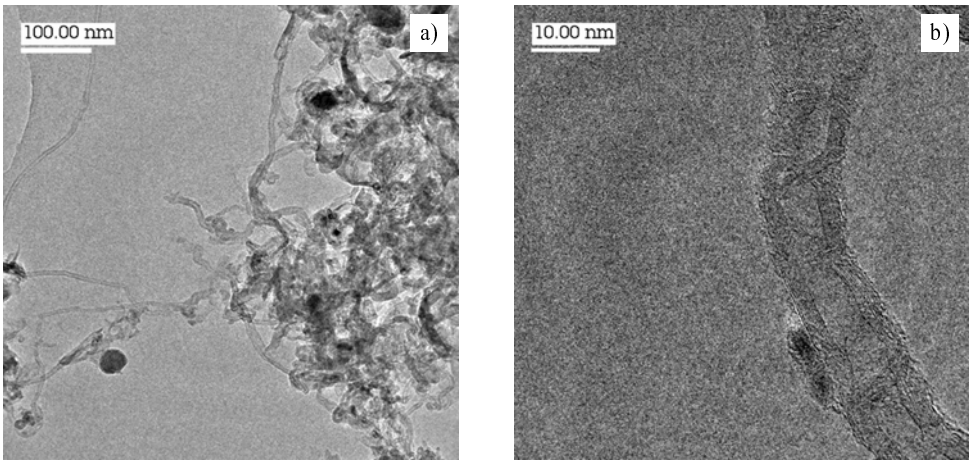

Fig. 5. HRTEM images of the sample carburised at 550 °C and then reduced at 450 °C (see the text for details)

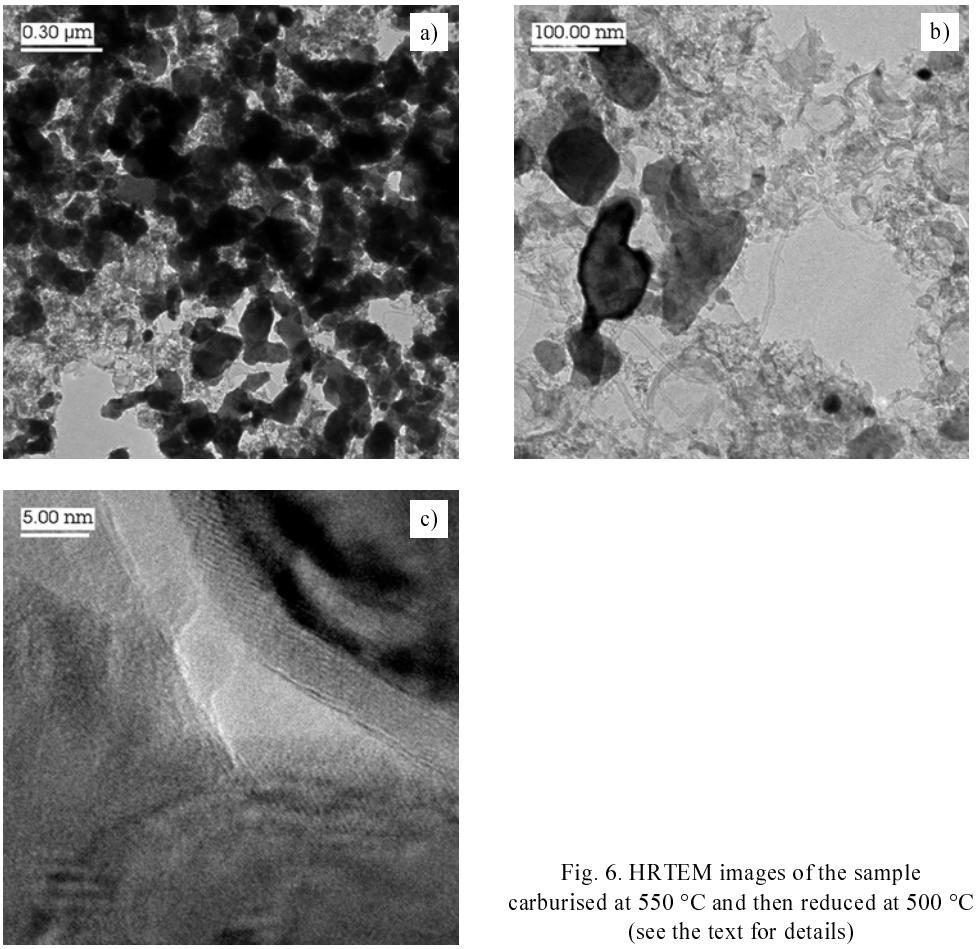

Fig. 6. HRTEM images of the sample carburised at 550 °C and then reduced at 500 °C (see the text for details)

After the hydrogenation of the same carburised sample at a higher temperature (500 °C), a further mass decrease was observed, until 0.2 g C/g Fe (sample I). The TG line corresponding to this hydrogenation process is shown in Fig. 1. As in the case of sample II, only the phase of α-Fe was detected by XRD analysis; then all iron carbide was reduced to iron. The increase of the iron concentration in carbon matrix is clearly visible in Fig. 6a (compared with Fig. 3a). The particles of iron are well dispersed, contrary to the pristine iron sample (an alloy) before carburisation. Thin carbonaceous forms can be seen in Fig. 6b. Simultaneously, as can be seen in Fig. 6c, the thickness of the graphitic layer after hydrogenation is lower (below 5 nm) than that after carburisation (about 15 nm, Fig. 3b).

Figure 7a presents the FMR spectra of all three samples, recorded at room temperature. In all spectra, a strong shift of the resonance lines in the direction of low magnetic field is observed. Intense FMR lines are broader than weaker ones. The obtained FMR spectra have shown a similarity to the FMR spectra of iron carbide and α-

iron [16-18]. The spectra of samples I and II are dominated by a line produced by α-iron, while the spectrum of the sample III is dominated by carbide iron. The fitting

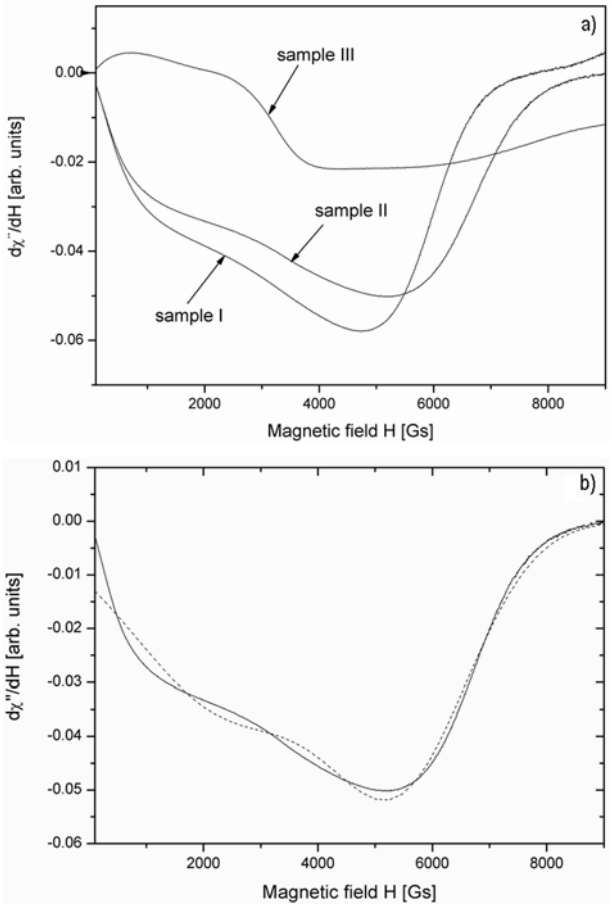

Fig. 7. FMR spectra of the samples: I – carburised at 550 °C followed by reduction at 500 °C; II – carburised at 550 °C followed by reduction at 450 °C; III – carburised at 550 °C (a); and the fitted FMR spectrum (dotted line) for sample II (b)

of the extended resonance absorption signals has been performed using Lorentzian -type curves taking into account absorption at both H_r and $-H_r$, induced by two oppositely rotating components of the linearly polarized radio-frequency incoming experimental field. The resonance absorption lines for samples I and II were fitted with two Lorentzian curves, one centred on the magnetic field near zero and the other at a higher field (Fig. 7b). Table 1 gives the values of FMR spectral parameters. Despite of this crude approximation, the results of the fitting could give a satisfactory explanation of the experimental results [18]. The results of the FMR measurements of the carburised and reduced samples are summarised in Table 1.

Table. 1. FMR parameters of the carburised and hydrogenated samples.

Sample	Composition	I_1 [a. u.]	ΔH_1 [mT]	H_{r1} [mT]	I_2 [a. u.]	ΔH_2 [mT]	H_{r2} [mT]
I, reduced at 500 °C	Fe+C, 0.2 g C/g Fe	5.8	410(1)	190(1)	2.7	184(30)	62(20)
II, reduced at 450 °C	Fe+C, 0.4 g C/g Fe	5.0	310(1)	210(1)	1.5	180(10)	~0
III, carburised	Fe_3C+C, 1.2 g C/g Fe	0.5	140(4)	250(3)	3	789(10)	35(10)

The FMR lines could originate mainly from ferromagnetic iron ions with their individual spins coupled by the exchange interaction within each nanoscale metallic grain. The iron ion with localised spins forming non-separated ferromagnetic nanoparticles is subject to magnetic field produced by the following interaction processes:

$$H_{tot} = H_{dem} + H_{dip} + H_{ex} \tag{1}$$

which could change the resonance condition:

$$h\nu = g\mu_B(H_{ex} \pm H_{in}) \tag{2}$$

where h is the Planck constant, μ_B is the Bohr magneton, H_{ex} is the applied external magnetic field, H_{in} is the internal magnetic field, H_{dip} is the magnetic dipole field from the neighbouring nanoparticles or agglomerates, H_{dem} is the so-called demagnetising field.

FMR spectra of the samples I and II are dominated by the signal arising from α-iron. The spectrum of the sample I is more intense in comparison to the sample II and the resonance field is more shifted to lower magnetic field. Despite of carburization of the sample III, iron carbide is a dominating phase while in the sample II produced at a lower hydrogenation temperature, the α-iron content is increased so that iron carbide is not observed by XRD measurements (Fig. 2). Essential changes in magnetic interaction are observed among the investigated samples influencing the values of the linewidth and intensity of the FMR spectrum (Fig. 7a). Increasing temperature of the hydrogenation process (about 50 K) decreases the carbon mass or increase the concentration of α-iron. The FMR spectrum of the sample III is dominated by iron carbide (Fig. 7a) which produces a characteristic very wide FMR line. Nanocrystalline α-iron forming conglomerates could create stronger magnetic field and magnetic interactions essentially influence the values of the FMR parameters, especially the linewidth and position of the resonance field.

4. Conclusions

Three samples of nanocrystalline iron were obtained, carburised with ethylene and subsequently reduced with hydrogen. After the treatment of the sample with hydrogen at 450 °C iron carbide is reduced to α-iron, which is reflected in FMR spectra. The

amount of carbon is reduced from 1.2 to 0.4 g C/g Fe which corresponds to the elimination of amorphous carbon and thick carbon nanofibres. After the reduction under hydrogen at 500 °C, the remaining mass of carbon of 0.2 g C/g Fe corresponds to thin multiwall carbon nanotubes. The FMR spectrum of this sample corresponds to an increased amount of iron. Changes of concentration of magnetic nanocrystallites strongly influences the FMR spectra. The position of the resonance line depends strongly on the concentration of magnetic nanocrystalline agglomerates suggesting that the dipole–dipole interaction could play an essential role in the magnetic interactions.

Acknowledgements

This work was partially supported by the grant PBZ-KBN-095/TO8/2003.

References

[1] BI X-X., GANGULY B., HUFFMAN G.P., HUGGINS F.E., ENDO M., EKLUND P.C., J. Mater. Res., 8 (1993), 1666.
[2] ZHAO X.Q., LIANG Y., HU Z.Q., LIU B.X., J. Appl. Phys., 80 (1996), 5857.
[3] GRIMES C.A., HORN J.L., BUSH G.G., ALLEN J.L., EKLUND P.C., IEEE Trans. Magn., 33 (1997), 3736.
[4] GRIMES C.A., QIAN D., DICKEY E.C., ALLEN J.L., EKLUND P.C., J. Appl. Phys., 87 (2000), 5642.
[5] DENES F.S., MANOLACHE S., MA Y.C., SHAMAMIAN V., RAVEL B., PROKES S., J. Appl. Phys., 94 (2003), 3498.
[6] GOODWIN T.J., YOO S.H., MATTEAZZI P., GROZA J.R., Nanostruct. Mater., 8 (1997), 559.
[7] YUMOTO H., NAGAMINE Y., NAGAHAMA J., SHIMOTOMAI M., Vacuum, 65 (2002), 527.
[8] VENEGONI D., SERP P., FEURER R., KIHN Y., VAHLAS C., KALCK P., Carbon, 40 (2002), 1799.
[9] QIAN W., LIU T., WANG Z., YU H., LI Z., WIE F., LUO G., Carbon, 41 (2003), 2487.
[10] QIAN W., LIU T., WEI F., WANG Z., LI Z., App. Catal. A: General, 258 (2004), 121.
[11] GULINO G., VIEIRA R., AMADOU J., NGUYEN P., LEDOUX M.J., GALVAGNO S., CENTI G., PHAM-HUU C., App. Catal. A: General, 279 (2005), 89.
[12] BOUGRINE A., NAJI A., GHANBAJA J., BILLAUD D., Synth. Met., 103 (1999), 2480.
[13] SHI Z., LIAN Y., ZHOU X., GU Z., AHANG Y., IIJIMA S., Solid State Comm., 112 (1999), 35.
[14] ZHANG Y., SHI Z., GU Z., IIJIMA S., Carbon, 38 (2000), 2055.
[15] IVANOV V., FONSECA A., NAGY J.B., LUCAS A., LAMBIN P., BERNAERTS D., ZHANG X.B., CARBON, 33 (1995), 1727.
[16] NARKIEWICZ U., GUSKOS N., ARABCZYK W., TYPEK J., BODZIONY T., KONICKI W., GASIOREK G., KUCHAREWICZ I., ANAGNOSTAKIS E.A., Carbon, 42 (2004), 1127.
[17] GUSKOS N., ANAGNOSTAKIS E.A., TYPEK J., GASIOREK G., BODZIONY T., NARKIEWICZ U., ARABCZYK W., KONICKI W., Mol. Phys. Rep., 39 (2004), 58.
[18] GUSKOS N., TYPEK J., NARKIEWICZ U., MARYNIAK M., AIDINIS K., Rev. Adv. Mat. Sci., 8 (2004), 10.
[19] GUSKOS N., ANAGNOSTAKIS E.A., LIKODIMOS V., BODZIONY T., TYPEK J., MARYNIAK M., NARKIEWICZ U., KUCHAREWICZ I., J. Appl. Phys., 97 (2005), 024304.
[20] NARKIEWICZ U., ARABCZYK W., KONICKI W., PATTEK-JAŃCZYK A., J. Mater. Res., 20 (2005), 386.

Received 9 September 2005
Revised 25 November 2005